

Spectral variability of the 3C 390.3 nucleus for more than twenty years. I. Variability of the broad and narrow emission-line fluxes

S. G. Sergeev,^{*} S. V. Nazarov, G. A. Borman

Crimean Astrophysical Observatory, P/O Nauchny Crimea 298409, Russia

28 November 2016

ABSTRACT

We summarize results of the analysis of the optical variability of the continuum and emission-line fluxes in the 3C 390.3 nucleus during 1992–2014. The [O III] $\lambda 5007$ flux increases monotonically by ≈ 30 per cent in 2003–2014. The narrow Balmer lines show similar monotonic increase, while the variability patterns of the [O I] $\lambda 6300$ narrow line are completely different from that of [O III]. The reverberation lags are found to be 88.6 ± 8.4 , 161 ± 15 , and 113 ± 14 d for the H β , H α , and H γ broad emission-lines, respectively. The reverberation mass of the central black hole equals to $(1.87 \pm 0.26) \times 10^9 M_\odot$ and $(2.81 \pm 0.38) \times 10^9 M_\odot$, for the H β and H α lines and assuming a scaling factor that converts the virial product to a mass to be $f = 5.5$. A difference between both masses can point to a difference between kinematics of the H α and H β emission regions. We show that the reverberation mapping can only be applied to the entire period of observations of the 3C 390.3 nucleus after removing a long-term trend. This trend has been expressed by a slowly varying scale factor $c(t)$ in the power-law relationship between the line and continuum fluxes: $F_{line} \propto c(t) F_{cont}^a$. We find the power-law index a equals to 0.77 and 0.54 for the H β and H α lines, respectively. The observed relationship between the Balmer decrement and the optical continuum flux is as follows: $F(\text{H}\alpha)/F(\text{H}\beta) \propto F_{cont}^{-0.20}$ and $F(\text{H}\beta)/F(\text{H}\gamma) \propto F_{cont}^{-0.18}$. The 3C 390.3 nucleus is an ‘outsider’ in the relationship between optical luminosity and black hole mass. Its Eddington ratio is $E_{bol}/E_{Edd} = 0.0037$.

Key words: galaxies: active – galaxies: nuclei – galaxies: Seyfert – quasars: emission lines – quasars: individual: 3C 390.3

1 INTRODUCTION

Photoionization by central source radiation in active galactic nuclei (AGN) is believed to be a main mechanism responsible for the gas emission in the broad-line region (BLR). So, the observed correlations between broad-line properties and continuum properties provides information necessary to develop photoionization models of the BLR. These models together with the observed line intensities and line intensity ratios are used to recover physical conditions in the BLR. The size, geometry, and kinematics of the BLR can be determined from the line-continuum correlation by the reverberation mapping technique (Blandford & McKee 1982; Peterson 1993, 1994). The most obvious success in the reverberation mapping studies is determination the BLR size for a lot of AGNs via the cross-correlation function. This function is applied to the light curves of the continuum and emis-

sion lines to find delays between variations of their fluxes (e.g., Peterson et al. 1998b; Kaspi et al. 2000; Bentz et al. 2010; Denney et al. 2010; Grier et al. 2012). Such studies require a good sampling of observations as well as significant variability amplitude with at least one event clearly seen in the continuum light curve. With the known BLR sizes and under some assumptions (such as virialized gas motion in the BLR), it is possible to determine the fundamental AGN characteristics – the central black hole mass and accretion rate (e.g., Peterson et al. 2004; Bentz et al. 2009).

Recent years, good progress has been achieved in applying the reverberation method to individual profile segments of the broad emission lines (e.g., Denney et al. 2009; Grier et al. 2012; Doroshenko et al. 2012). These reverberation results suggest that the BLR kinematics can be distinctly different (inflow, outflow, or virialized motions) for individual AGNs.

The line emission from the narrow-line region (NLR) is believed to be constant in flux during several decades

^{*} E-mail: sergeev.crao@mail.ru

because this region is very extended spatially (hundreds of light years). However, some authors have claimed the narrow-line variability for a shorter period. For example, Pronik & Pronik (1992) have carefully assumed that “Time scale variability in most cases is several years, but months and weeks should not be excluded” for the $[\text{O III}] \lambda\lambda 5007, 4959 \text{ \AA}$ forbidden lines in some nuclei. Peterson et al. (2013) have found that “The narrow $[\text{O III}] \lambda\lambda 5007, 4959$ emission-line fluxes in the spectrum of the well-studied Seyfert 1 galaxy NGC 5548 are shown to vary with time.” and they suggested the size of the $[\text{O III}]$ -emitting region in NGC 5548 to be 1–3 pc. Zheng et al. (1995) have studied the intensities of the narrow lines in 3C 390.3 between 1974 and 1990. They have found the flux of $[\text{O III}] \lambda 4959$ has declined by 40 per cent between 1974 and 1984. It has remained at a low level between 1984 and 1987, and then increased to a higher level since 1988, in step with the long-term variation of the underlying optical continuum. In most papers, the light curves of the continuum and broad emission lines are calculated using narrow line intensities as ‘photometric standards’. Therefore, narrow line variability over a period of observations leads to the appearance of fictive longtime ‘trends’ in the derived light curves.

The 3C 390.3 nucleus is often considered as a prototype for a relatively small group of AGNs (referred to as ‘double-peaked emitters’) with broad and double-peaked low-ionization lines in their spectra. The Balmer emission lines in the optical spectrum of the 3C 390.3 nucleus are very broad with strong blueshifted and redshifted peaks that have been well known long time ago (e.g., Sandage 1966; Lynds 1968; Burbidge & Burbidge 1971). It is one of the best studied nucleus among double-peaked emitters (e.g., Osterbrock, Koski & Phillips 1976; Barr et al. 1980; Yee & Oke 1981; Netzer 1982; Veilleux & Zheng 1991; Zheng 1996; Wamsteker et al. 1997; Dietrich et al. 1998; O’Brien et al. 1998; Shapovalova et al. 2001; Sergeev et al. 2002; Gezari, Halpern & Eracleous 2007; Shapovalova et al. 2010; Sergeev et al. 2011; Dietrich et al. 2012; Afanasiev et al. 2015).

Among various BLR models, the disc-like BLR around the central black hole is widely accepted to explain the broad emission-line profiles in double-peaked emitters. Double-peaked broad lines being well fitted by the emission from the relativistic circular accretion disc within a distance from the black hole of hundreds to thousands of gravitational radii (Chen & Halpern 1989; Chen, Halpern & Filippenko 1989). Modifications of this model include an elliptical accretion disc model (Eracleous et al. 1995), a stochastically perturbed accretion disc model (Flohic & Eracleous 2008), a system of clouds rotating predominantly in the same plane (Sergeev, Pronik, & Sergeeva 2000), etc. However, the BLR geometry in 3C 390.3 seems to be very complex with at least two components, although the disc-like component is, probably, the dominant emitter (Sergeev et al. 2002; Shapovalova et al. 2010; Afanasiev et al. 2015).

There is some inconsistency among published lag measurements in 3C 390.3. The lag between the continuum and Balmer emission-line variations was found to be ≈ 90 –180 days from the long-term (several years) monitoring campaigns (Shapovalova et al. 2001; Sergeev et al. 2002; Shapovalova et al. 2010; Sergeev et al. 2011; Afanasiev et al. 2015), more than twice the lag found

from the short-term campaigns (Dietrich et al. 1998, 2012). A summary of the lag estimates is given in Kovačević et al. (2014).

The present study is the continuation of the previous studies of 3C 390.3 nucleus carried out in the Crimean Astrophysical Observatory (CrAO) since 1992 (Sergeev et al. 2002, 2011). Now we present new results of the optical spectroscopic observations of 3C 390.3 during monitoring campaign from 2008 to 2014 and we summarize the results obtained on 3C 390.3 in 1992–2014. The main goals of the present paper are similar to that of Sergeev et al. (2011): (1) To determine the BLR size and the black hole mass via reverberation mapping technique; (2) To check for the narrow-line variability; and (3) To determine power-law indices of the relationship between Balmer line and continuum fluxes and to look for any changes in the Balmer decrement. The structure of the present paper is similar to the paper of Sergeev et al. (2011).

We analyze the total line fluxes only, not the line profiles. In the next papers of this series we plan to study variations of individual profile segments of the broad Balmer lines, including the 2-d reverberations mapping and the long-term evolution of the broad emission-line profiles. We hope our results will be used to critically test competing models of the double-peaked emitters.

2 OBSERVATIONS AND DATA REDUCTION

2.1 Optical spectroscopy

Optical spectra of 3C 390.3 have been obtained at the 2.6-m Shajn telescope of the CrAO since 1992. The results of the observations for the periods 1992–2000 and 2001–2007 are published in Sergeev et al. (2002, 2011). The spectra were registered at the two separate spectral regions centered at the $\text{H}\alpha$ and $\text{H}\beta$ lines. Since July 2005 the old Astro-550 CCD was replaced by a more modern SPEC-10 CCD. More details about observations, observational setup, and spectral data processing are in Sergeev et al. (2002, 2011).

Our new data set in 2008–2014 consists of 96 spectra in the $\text{H}\beta$ region and 30 spectra in the $\text{H}\alpha$ region. The signal-to-noise ratio (S/N) per pixel at the continuum level is in the range 21–109 (mean value is 51) for the $\text{H}\beta$ region and in the range 31–79 (mean value is 50) for the $\text{H}\alpha$ region.

The spectra of the 3C 390.3 nucleus have been calibrated in flux as described in Sergeev et al. (2002). The final step of this calibration is the scaling of spectra to match the fluxes of the selected narrow emission lines which are assumed to be constant over time-scales of the monitoring programme. This assumption is justified by the large spatial extent of the narrow line region (NLR). In the case of 3C 390.3 the underlying difficulty is that there is some evidence for narrow-line variability (Clavel & Wamsteker 1987; Zheng et al. 1995; Sergeev et al. 2011). We discuss this problem in section 2.2.

We chose the narrow $[\text{O III}] \lambda 5007$ ($\text{H}\beta$ region) and $[\text{O I}] \lambda 6300$ ($\text{H}\alpha$ region) emission lines as internal flux standards. Their absolute fluxes were measured from the spectra obtained under photometric conditions by using the spectra of the comparison star (see Sergeev et al. 2002).

As in Sergeev et al. (2002, 2011) the line fluxes were

measured by integrating the flux above the underlying continuum within the selected wavelength intervals. The continuum fluxes were determined at 5100Å and 6200Å in the rest frame of 3C 390.3, and designated them as F_{5100} and F_{6200} , respectively.

The uncertainties in our H α -region fluxes are much greater than in the H β -region ones because they are dominated by the uncertainties in the flux-scaling factors determined from the relatively weak [O I] λ 6300 narrow line.

2.2 Optical photometry

Regular CCD photometric observations of the selected AGNs have been started at the CrAO in 2001. The instrumentation, reductions and measurements of our photometric data are described in Doroshenko et al. (2005) and Sergeev et al. (2005).

Our V filter photometric measurements of 3C 390.3 were calibrated to match the F_{5100} continuum fluxes as described in Sergeev et al. (2011), namely:

$$F_{5100} = \varphi (10^{-0.4V} - G), \quad (1)$$

where V is the stellar magnitude corrected for the broad H β line, φ is a scale factor, and G is a difference in constant contributions (host galaxy and NLR). The parameters φ and G were determined by the ordinary linear regression. Just the same as in Sergeev et al. (2011) we have found strong discrepancy in our spectral and photometric measurements that can only be removed by assuming long-term changes in the scale factor φ . Now we have enough absolute measurements of the [O III] λ 5007 Å line fluxes made using the comparison star during nights with good weather conditions to prove that above changes must be attributed to the narrow-line variability. We present the results on this variability in section 3.2. So, in contrast to Sergeev et al. (2011), we assumed that our photometric measurements are correct, while our spectral measurements are wrong because variability of the narrow lines. To correct our spectral measurement we recovered $\varphi(t)$ function as described in Sergeev et al. (2011). We selected it to be a small degree polynomial function of time. The polynomial coefficients and offset G were determined by achieving the best rms agreement between photometric and spectral data sets. We adopted the $\varphi(t)$ function to be constant ($\varphi = \varphi_0$) before beginning of the systematic continuum brightening in \approx 2003. Total of 105 data points were used for the fit. The best fit normalized function $\varphi(t)/\varphi_0$ is shown in Fig. 1. It was computed for the degrees of polynomial function from 1 to 4. The $\varphi(t)$ function is very similar for all polynomial degrees and it increases monotonically by \approx 30 per cent during about ten years. The best solution for the polynomial degree 3 is as follows:

$$\frac{\varphi(t)}{\varphi_0} = \begin{cases} 0.8790 - 0.07324 \Delta t + 0.002255 \Delta t^2 + \\ 0.004117 \Delta t^3, \text{ for } t > 2452472.5 \\ 1, \text{ for } t \leq 2452472.5 \end{cases} \quad (2)$$

where Δt is adopted to be $\frac{t-2454713.1}{1000}$, t is Julian Date, and φ/φ_0 is adopted to be 1 before JD2452472.5, i.e., before beginning of the systematic continuum brightening. The time of 2454713.1 is simply the averaged value of t , so we adopt $\Delta t = 0$ for the mean time t .

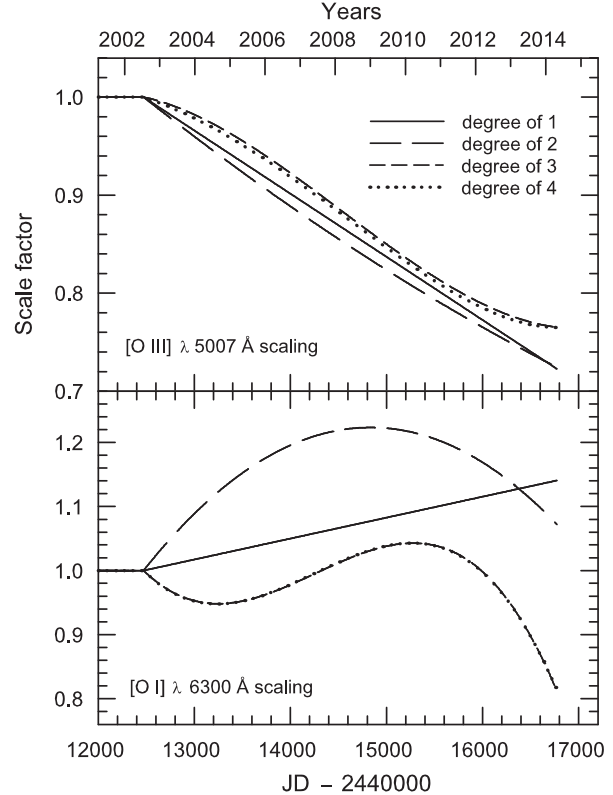


Figure 1. Normalized scale factor φ as a polynomial function of time to scale our V filter photometry to match the F_{5100} (top panel) and F_{6200} (bottom panel) continuum fluxes. The legend for polynomial degrees is shown in the top panel. The φ is adopted to be 1 before JD2452472.5.

However, the same method applied to the H α -region spectra (scaled using [O I] λ 6300Å narrow line) gives ambiguous result (see Fig. 1, bottom panel) where the recovered $\varphi(t)$ functions are too different for various polynomial degrees. Absolute flux measurements of the [O I] λ 6300Å line (see section 3.2) show different variability patterns and smaller variability amplitude as compared to the [O III] λ 5007 Å. Because our results on the [O I] variability as well as on the $\varphi(t)$ function recovery are too unreliable, our H α -region fluxes were not corrected for the narrow-line variability.

The reliability of the $\varphi(t)$ fit for the [O III] λ 5007 line (as well as its unreliability for the [O I] λ 6300 line) is clearly seen from Table 1 where fractional rms agreement (corrected for degree-of-freedom) between spectral and photometric data sets are shown. In particular, the assumptions that the $\varphi(t)$ for the [O III] λ 5007 is a straight line improves the rms agreement by 3 times, while the same assumption for the [O I] λ 6300 line does not improve it any significantly.

2.3 Final light curves

As mentioned in the previous section, we found that our photometric V -band measurements are correct, while our continuum light curve F_{5100} has a long-term trend because long-term flux changes in the [O III] λ 5007 line used for cali-

Table 1. Quality of the $\varphi(t)$ function fit given as a fractional rms agreement (in per cents) between spectral and photometric data sets

Calibration line	rms agreement for polynomial degree of				
	0	1	2	3	4
[O III] $\lambda 5007$	6.984	2.375	2.338	2.286	2.285
[O I] $\lambda 6300$	5.277	5.258	4.875	4.445	4.449

Table 2. $H\beta$ region fluxes. This is a sample of the full table, which is available online.

Julian Date -2,440,000	F_{5100}	$H\beta$	$H\gamma$
14480.199	42.28 \pm 0.44	33.77 \pm 0.70	13.06 \pm 0.78
14483.202	43.98 \pm 0.44
14497.173	44.46 \pm 0.35
14503.206	44.25 \pm 0.49
14508.652	42.89 \pm 0.72	34.30 \pm 0.86	11.39 \pm 0.93

Units are 10^{-14} ergs cm $^{-2}$ s $^{-1}$ and 10^{-16} ergs cm $^{-2}$ s $^{-1}$ Å $^{-1}$ for the lines and continuum, respectively. The fluxes are consistent with the respective fluxes for earlier period (Sergeev et al. 2011) when both the fluxes and uncertainties from Sergeev et al. (2011) are divided by the scale factor $\varphi(t)$ (see text).

bration of the $H\beta$ -region spectra. To merge the photometric and spectral data sets we have first put the photometric light curve into the scale of the continuum spectral fluxes (ergs cm $^{-2}$ s $^{-1}$ Å $^{-1}$) by subtracting an offset G and by multiplying by a factor $\varphi = \varphi_0$. Then the spectral fluxes (F_{5100} , $H\beta$, and $H\gamma$) were corrected for the narrow-line variability by dividing them by $\varphi(t)/\varphi_0$ (see eq. 2). Because of this correction, some values quoted in the present paper may differ slightly from those in Sergeev et al. (2011). The joined continuum light curve has been nightly averaged.

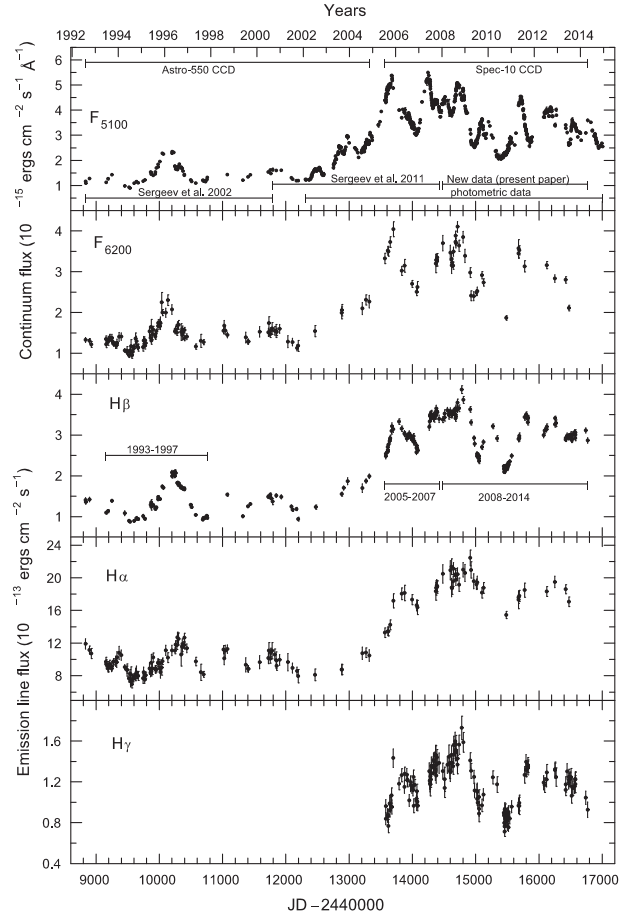
We do not perform any corrections for the $H\alpha$ -region fluxes because our results on the [O I] $\lambda 6300$ variability are too unclear.

The fluxes with their observational uncertainties are shown in Fig. 2 for 1992–2014. They are presented in Tables 2 and 3 for 2008–2014. Note, that the F_{5100} continuum flux consists of both the spectral and photometric data. The fluxes for earlier period are given in Sergeev et al. (2002, 2011). However, the $H\beta$ -region fluxes from Table 1 of Sergeev et al. (2011) must be corrected for the narrow-line variability (i.e., divided by the factor $\varphi(t)/\varphi_0$, see eq. 2) to be consistent with the fluxes for 2008–2014 from Table 2 of the present papers. Note that we have not separated the broad and narrow line fluxes. Because narrow line fluxes are shown to be variable, they must slightly affect the variability of the broad lines. However, we found this effect to be negligible (not more than 2 per cent).

3 RESULTS

3.1 Variability characteristics

The basic variability characteristics of 3C 390.3 are summarized in the Table 4. We considered the four periods of observations: 1993–1997, 2005–2007, 2008–2014, and the entire

**Figure 2.** Light curves (top to bottom) for the continua at $\lambda 5100\text{\AA}$ and $\lambda 6200\text{\AA}$ and for the $H\beta$, $H\alpha$, and $H\gamma$ lines. Units are 10^{-13} ergs cm $^{-2}$ s $^{-1}$ and 10^{-15} ergs cm $^{-2}$ s $^{-1}$ Å $^{-1}$ for the lines and continua, respectively.

period of CCD observations of 3C 390.3 at the CrAO (1992–2014). The motivation of the division of the data into the periods is that the first two periods were used for the cross-correlation analysis in Sergeev et al. (2002, 2011). The 1998–2004 period has been excluded from the cross-correlation analysis because poor data sampling of both the $H\beta$ and $H\alpha$ lines, while 2008–2014 period represents our new (unpublished) data. On the other hand, this division can be used to check for lag changes. In the Table 4 the parameter F_{var} is the rms fractional variability and the parameter R_{max} is simply the ratio of the maximum to minimum flux. Both the parameters are corrected for observational uncertainties. We also give the variability characteristics corrected for the contribution of the starlight of the host galaxy in the case of the continuum and the narrow-line contamination in the case of the emission lines (for our estimates of these contributions see table 1 and text in Sergeev et al. 2002). We accounted for the long-term trends in the narrow-line variability when subtracting narrow-line contamination from the broad-line fluxes (see sect. 2.2 and 3.2 for more details).

The considered variability characteristics for any light curve can only be compared to another light curve when both of them are sampled identically. However, there are a notable difference in the sampling of our $H\alpha$ -region and

Table 3. H α region fluxes in the two wavelength windows: 6740–7160 Å and 6777.0–7033.5 Å (observer frame).

Julian Date -2,440,000	F_{6200}	H α 6740–7160 Å	H α 6777.0–7033.5 Å
14481.250	37.00 \pm 1.92	204.9 \pm 11.3	173.6 \pm 9.4
14600.422	34.66 \pm 1.86	209.2 \pm 11.7	175.7 \pm 9.7
14617.480	33.07 \pm 1.39	213.6 \pm 9.6	179.4 \pm 7.9
14620.523	31.54 \pm 1.93	188.1 \pm 11.4	157.8 \pm 9.4
14625.422	32.23 \pm 1.14	187.1 \pm 7.4	157.9 \pm 6.1
14643.512	31.50 \pm 0.88	195.7 \pm 6.4	164.9 \pm 5.1
14650.441	34.93 \pm 1.09	211.1 \pm 7.6	177.6 \pm 6.1
14681.379	37.30 \pm 0.96	203.0 \pm 6.5	171.6 \pm 5.2
14683.445	38.83 \pm 1.12	204.3 \pm 7.1	173.3 \pm 5.8
14687.367	37.00 \pm 1.14	197.7 \pm 7.2	166.9 \pm 5.8
14714.395	41.03 \pm 1.30	204.3 \pm 7.8	172.9 \pm 6.3
14738.270	36.39 \pm 1.38	191.5 \pm 8.2	161.6 \pm 6.7
14802.266	38.48 \pm 1.42	209.9 \pm 8.8	177.3 \pm 7.2
14833.188	33.89 \pm 1.62	205.9 \pm 10.5	174.4 \pm 8.7
14912.594	29.79 \pm 1.21	224.5 \pm 9.7	189.7 \pm 8.0
14927.488	24.13 \pm 1.20	209.6 \pm 10.0	176.8 \pm 8.3
14969.477	24.01 \pm 1.10	195.8 \pm 9.2	165.7 \pm 7.6
15010.508	24.90 \pm 0.76	192.0 \pm 6.3	161.3 \pm 5.1
15024.430	25.26 \pm 0.98	194.3 \pm 7.7	162.8 \pm 6.3
15098.344	29.15 \pm 0.90	181.8 \pm 6.4	151.2 \pm 5.1
15124.367	27.37 \pm 0.86	187.7 \pm 6.5	156.9 \pm 5.3
15482.258	18.69 \pm 0.53	154.4 \pm 4.5	127.5 \pm 3.6
15676.539	34.48 \pm 1.21	175.9 \pm 7.1	145.7 \pm 5.7
15677.555	35.72 \pm 2.17	173.1 \pm 11.1	143.7 \pm 9.0
15689.504	35.25 \pm 1.12	177.9 \pm 6.7	147.8 \pm 5.3
15772.469	31.32 \pm 1.37	185.0 \pm 8.7	155.0 \pm 7.1
16122.402	31.61 \pm 0.90	183.3 \pm 6.2	154.2 \pm 4.9
16252.246	28.34 \pm 0.93	194.9 \pm 7.0	162.3 \pm 5.7
16422.424	28.02 \pm 0.78	186.1 \pm 5.6	154.9 \pm 4.5
16472.480	21.11 \pm 0.70	170.7 \pm 5.8	140.6 \pm 4.7

Units are 10^{-14} ergs cm $^{-2}$ s $^{-1}$ and 10^{-16} ergs cm $^{-2}$ s $^{-1}$ Å $^{-1}$ for the lines and continuum, respectively. H α fluxes in the last column of this table were integrated over the same line-of-sight velocities as for H β .

H β -region light curves. To avoid effect of sampling we have selected quasi-simultaneous data points from both regions to construct the identically sampled light curves. Their variability characteristics are given in the last five rows of the Table 4. As can be seen from these rows, the fractional variability amplitude is almost the same for the continuum fluxes at $\lambda 5100$ and $\lambda 6200$ (probably it is slightly greater for $\lambda 5100$). Among observed Balmer lines, the variability amplitude is greatest in H γ , less in H β , and lowest in H α .

3.2 Narrow-line variability

The discrepancy between our spectral and photometric data sets (sect. 2.2) can be attributed to the long-term variability of the [O III] $\lambda 5007$ Å forbidden line. If so, the light curve of the [O III] line must be inversely proportional to the scale factor $\varphi(t)$ that was determined in sect. 2.2. To check the narrow-line variability in 3C 390.3 the narrow-line fluxes were computed for photometric nights using the absolute flux calibration by the comparison star. To reduce some contribution from the far red wing of the H β line to the [O III] line and from the far blue wing of the H α line to the [O I] $\lambda 6300$ line we selected a slightly narrower integra-

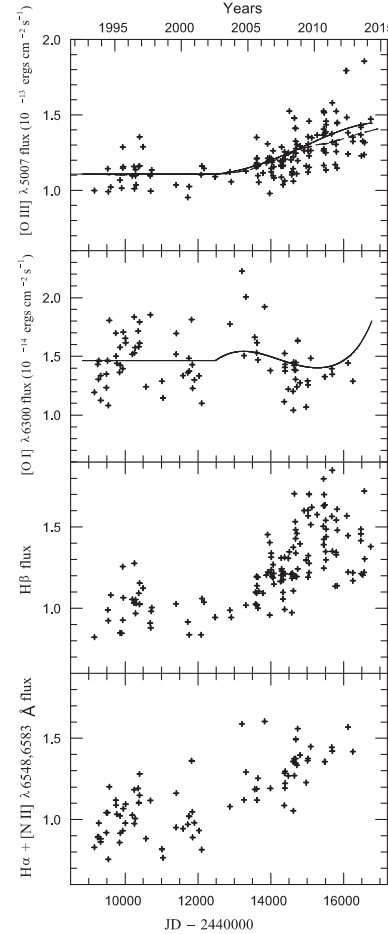


Figure 3. Shown by the crosshair symbols are the light curves of the following narrow lines (top to bottom): [O III] $\lambda 5007$, [O I] $\lambda 6300$, H β , and H α + [N II] $\lambda\lambda 6548, 6583$. The narrow-line fluxes were computed from the spectra obtained under photometric conditions by using the spectra of the comparison star. Flux units in the last two panels are arbitrary. The suspected variations of the [O III] and [O I] lines according to the changes in the scale factor φ are shown by the solid lines, and the predicted variations in the [O III] line in terms of the model that is considered as an example in Sergeev et al. (2011) are shown by the dashed line.

tion zones for the narrow lines as compared to Sergeev et al. (2002, 2011) with closely adjacent pseudo-continuum windows (both red-side and blue-side windows for each line). The light curves of the [O III] and [O I] lines are shown in Fig. 3. Also given in Fig. 3 are inverse scale factors $\varphi(t)^{-1}$ for both lines.

We determined the probability that the observed narrow-line fluxes are proportional to $\varphi(t)^{-1}$ (alternative statistical hypothesis is that the narrow-lines do not vary in flux). We have found, from the χ^2 -criterion, that the constant flux hypothesis must be rejected at 0.94 and $1 - 1.4 \times 10^{-9}$ for the [O I] and [O III] lines, respectively. So, the confidence level for the correlation between narrow-line fluxes and $\varphi(t)^{-1}$ is almost 100 per cent for the [O III] line, but it is not significant enough for the [O I] line.

In Sergeev et al. (2011) it was shown that a shell model

Table 4. Variability characteristics.

Feature	1993–1997			2005–2007			2008–2014			1992–2014		
	Mean	F_{var}	R_{max}	Mean	F_{var}	R_{max}	Mean	F_{var}	R_{max}	Mean	F_{var}	R_{max}
F_{5100}	15.0	0.250	2.60	41.8	0.162	1.76	33.0	0.244	2.32	29.5	0.417	5.98
F_{5100}^*	10.3	0.365	4.38	37.1	0.182	1.90	28.3	0.285	2.68	24.8	0.496	11.50
$H\beta$	13.9	0.280	2.35	31.1	0.107	1.41	29.7	0.177	1.92	25.0	0.350	4.63
$H\beta^*$	12.7	0.308	2.56	29.6	0.112	1.43	28.0	0.188	2.00	23.5	0.366	5.18
$H\gamma$	11.7	0.140	1.71	11.7	0.192	2.16
$H\gamma^*$	9.4	0.169	1.95	9.0	0.255	2.80
F_{6200}	14.1	0.183	2.21	32.3	0.119	1.59	31.6	0.174	2.18	20.0	0.439	3.96
F_{6200}^*	7.10	0.363	4.48	25.3	0.151	1.82	24.6	0.223	2.89	13.0	0.675	9.57
$H\alpha$	94.2	0.138	1.65	168.1	0.124	1.33	193.8	0.068	1.42	124.1	0.353	2.94
$H\alpha^*$	83.8	0.155	1.76	155.9	0.131	1.35	179.8	0.077	1.47	112.7	0.377	3.20
F_{5100}^{**}	9.86	0.367	4.23	36.7	0.184	1.73	33.6	0.210	2.14	22.5	0.594	10.36
$H\beta^{**}$	12.1	0.309	2.54	29.4	0.123	1.36	31.2	0.112	1.59	21.4	0.453	4.86
$H\gamma^{**}$	9.4	0.227	2.06	10.5	0.168	1.69
F_{6200}^{**}	7.37	0.354	4.74	25.2	0.165	1.81	25.1	0.201	2.39	16.4	0.578	11.71
$H\alpha^{**}$	84.9	0.168	1.55	157.1	0.121	1.35	181.7	0.060	1.28	129.1	0.358	2.86

Units for the ‘Mean’ (mean flux) columns are the same as in the Tables 2 and 3. Rows marked with * or ** represent data with subtracted constant contributions. Rows marked with ** (last five rows) represent identically sampled light curves.

of the NLR with inner and outer radii of 20 and 200 light-years, respectively, and the emissivity per unit volume $\varepsilon \propto r^{-3.2}$ gives a good fit to the changes in the [O III] line flux (see their Fig. 3). Note that this model has been considered as an example, not a fit. It is remarkable that it gives a good prediction for the [O III] variability in 2008–2014 (top panel of Fig. 3). After several attempts we have found parameters of a shell models that provide an ideal fit to $\varphi(t)^{-1}$ with rms agreement to be less than one per cent, that is: inner and outer radii of 20 and 150 light-years, respectively, and the emissivity per unit volume $\varepsilon \propto r^{-3.5}$. We conclude that there are a lot of NLR models that is able to reproduce the observed [O III] variability.

The observed variability of the [O III] $\lambda 5007$ forbidden line strongly suggests that the narrow Balmer lines must be variable in flux as well. However, to measure fluxes of the narrow Balmer lines, they must be separated from the respective broad lines. Estimates of the narrow Balmer line fluxes were obtained via finding a scale factor for each spectrum to achieve a maximum smoothness of the residuals between a given spectrum and template spectrum (see calibration method by van Groningen & Wanders 1992, independently developed in the CrAO). In other words, there must be no narrow-line residuals seen over spectral region where these narrow lines reside when the template spectrum is subtracted from a given spectrum. As a criterion for smoothness we have selected the rms agreement between residuals for a given spectrum and smoothed version of these residuals (only for a spectral region where a given narrow line resides). To smooth residuals we have used a convolution with Π -shaped function with 24 Å full width (i.e., the function value is a positive number in the ± 12 Å interval, and it is zero outside this interval). The results for the $H\beta$ narrow line and for the $H\alpha + [\text{N II}]$ complex of narrow lines are shown in Fig. 3. It is clearly seen that above lines vary in flux and that these variations are similar to the [O III] line variations.

We have compared the variability amplitudes of the $H\beta$, $H\alpha + [\text{N II}]$, and [O III] narrow lines. We considered

long-term flux changes only, since a large short-term scattering of the observed narrow-line fluxes is the observational uncertainties. We found an rms amplitude to be about $F_{var} = 0.14$, and max-to-min variations to be a factor of $R_{max} = 1.6$ for both the $H\beta$ and $H\alpha + [\text{N II}]$ lines. The [O III] line shows smaller variability amplitude of $F_{var} = 0.083$ and $R_{max} = 1.36$.

We have experimented with various criteria for smoothness of the residuals (various widths of the Π -shaped kernel or low-order polynomial functions as a smoothed version of the residuals) and we found similar variability patterns of the $H\beta$ and $H\alpha + [\text{N II}]$ narrow lines with the same or slightly higher (up to a factor of 1.3) variability amplitudes.

Finally, in Fig. 4 we show the differences in fluxes between mean star-calibrated spectra S_1 , S_2 , and S_3 for the three periods: 1993–1997, 2005–2007, and 2008–2014, respectively ($S_2 - S_1$, $S_3 - S_1$, $S_3 - S_2$ flux differences are shown). The residuals in Fig. 4 clearly demonstrate many narrow-line features associated with the under-subtracted narrow lines. It proves that the narrow lines are indeed variable. It is clearly seen that most of the narrow lines in Fig. 4 are brighter in 2005–2007 than in 1993–1997, and brighter in 2008–2014 than in 2005–2007.

3.3 Time-series analysis

The time delays between various light curves were determined as in Sergeev et al. (2011), i.e., using the interpolation cross-correlation function (ICCF, e.g., Gaskell & Sparke 1986; White & Peterson 1994). The results of the cross-correlation analysis for 2008–2014 are shown in Table 5. Also given in Table 5 are the cross-correlation results from the previous Crimean studies: for 1993–1997 (Sergeev et al. 2002) and for 2005–2007 (Sergeev et al. 2011). The continuum- $H\beta$ CCFs for the considered periods are shown in Fig. 5.

The narrow-line variability leads to the appearance of fictive long-term trends in the derived light curves. The cross-correlation results as well as other results of the present

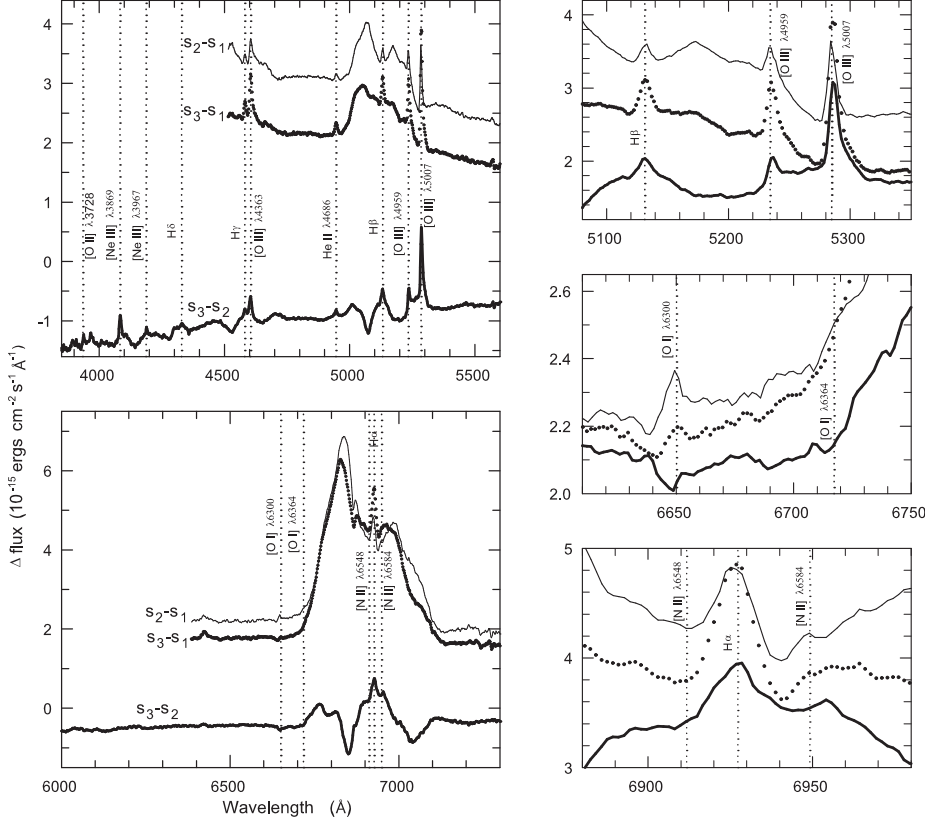


Figure 4. Residuals between mean star-calibrated spectra (S_1 , S_2 , and S_3) for 1993–1997, 2005–2007, and 2008–2014, respectively. The S_2 - S_1 , S_3 - S_1 , and S_3 - S_2 flux differences are shown by the thin solid line, filled circles, and thick solid line, respectively. Right panels show an enlarged portion of wavelengths near $H\beta$ and $[O III]\lambda 5007$ (top), $[O I]\lambda 6300, 6364$ (middle), and $H\alpha + [N II]$ (bottom). The residuals in the right panels are artificially shifted in Y-axis for better view. Dotted vertical lines indicate position of the strong narrow lines. Narrow-line features in the residuals are under-subtracted narrow lines.

Table 5. Cross-correlation results.

Series	1993–1997				2005–2007				2008–2014				Mean τ_{cent}
	τ_{peak}	τ_{cent}	r_{max}	P	τ_{peak}	τ_{cent}	r_{max}	P	τ_{peak}	τ_{cent}	r_{max}	P	
$F_{5100} - H\beta$	50^{+21}_{-2}	82^{+8}_{-8}	0.945	0	108^{+6}_{-11}	110^{+3}_{-9}	0.903	0	56^{+14}_{-1}	74^{+5}_{-3}	0.960	0	88.6 ± 8.4
$F_{5100} - H\alpha$	196^{+16}_{-79}	162^{+31}_{-12}	0.848	0	183^{+23}_{-40}	179^{+13}_{-20}	0.936	0	117^{+65}_{-5}	144^{+25}_{-26}	0.839	0.002	161 ± 15
$F_{5100} - H\gamma$	136^{+5}_{-12}	134^{+7}_{-11}	0.806	0	60^{+1}_{-7}	91^{+8}_{-7}	0.912	0	113 ± 14
$H\beta - H\alpha$	56^{+55}_{-3}	80^{+22}_{-13}	0.922	4×10^{-4}	49^{+66}_{-12}	82^{+26}_{-29}	0.972	0.005	51^{+62}_{-13}	72^{+49}_{-20}	0.843	0.003	78 ± 15
$H\beta - H\gamma$	37^{+8}_{-17}	32^{+25}_{-12}	0.925	0.011	19^{+16}_{-14}	16^{+13}_{-5}	0.947	0.010	24 ± 12
$F_{5100} - F_{6200}$	-8^{+11}_{-10}	-7^{+11}_{-12}	0.947	0.74	27^{+12}_{-26}	20^{+10}_{-14}	0.985	0.075	1^{+3}_{-5}	-5^{+5}_{-4}	0.970	0.82	2.6 ± 7.4

NOTE: P is a probability that τ_{cent} is less than zero. $H\alpha$ line fluxes are integrated over the same line-of-sight velocities as for $H\beta$.

paper are given with accounting for this trend for the $H\beta$ -region light curves ($H\beta$, $H\gamma$, and F_{5100}), including 2005–2007 period of observations. See sect. 2.2 and 3.2 for more details.

The lags were measured from both the location of the maximum value of the ICCF correlation coefficient (r_{max}) and from the ICCF centroid based on all points with $r \geq 0.8r_{max}$ (designated as τ_{peak} and τ_{cent} , respectively). The lag uncertainties were computed using the model-independent Monte Carlo flux randomization/random subset selection (FR/RSS) technique described by Peterson et al. (1998a). From this technique we have obtained the lag probability distributions. Fig. 6 shows prob-

ability distributions for τ_{cent} for both $H\beta$ and $H\alpha$ lines (respective lag measurements are in the first two rows of Table 5). We found that the lag for the $H\beta$ line in 2005–2008 is different from that in 1993–1997 and in 2008–2014 with a probability of 0.989 and 0.9997, respectively. We have conservatively attributed above difference to some additional lag uncertainty (see below). No significant difference in the $H\alpha$ lag among considered periods has been found.

Also given in Table 5 are unweighted mean lags for three periods of observations. The uncertainties in the mean lag were computed via maximum likelihood method in assumption that there is an internal lag scattering in addition

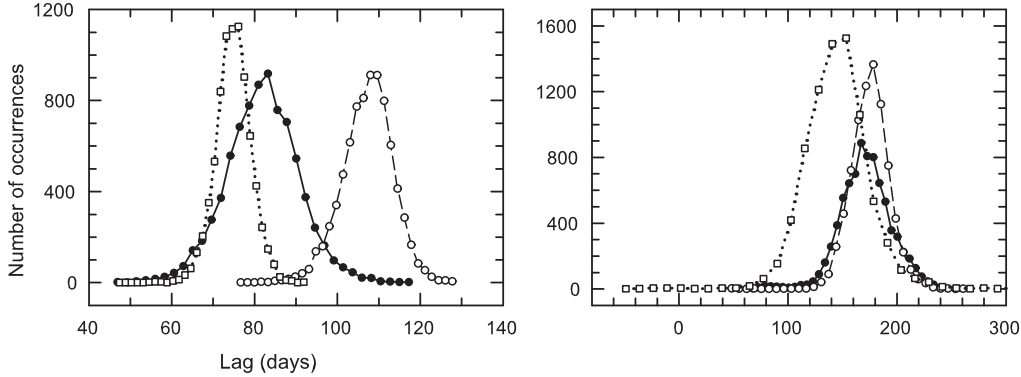


Figure 6. Probability distributions for a lag (τ_{cent}) between continuum and both H β (left panel) and H α (right panel) lines for 1993–1997 (filled circles connected by a solid line), 2005–2007 (open circles connected by a dashed line), and 2008–2014 (open squares connected by a dotted line). The distributions are derived from the FR/RSS technique.

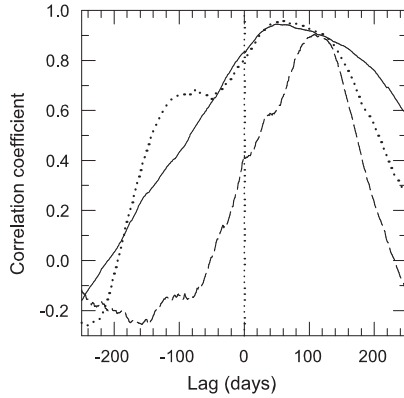


Figure 5. Continuum–H β cross-correlation functions for 1993–1997 (solid line), 2005–2007 (dashed line), and 2008–2014 (dotted line). Vertical dotted line indicates zero lag.

to the scattering derived from the FR/RSS technique for the individual observational periods. A reason to introduce this internal uncertainty is clearly seen from the Fig. 6: the computed probability distribution for the H β lag is too different between 2005–2007 and 2008–2014, so an additional uncertainty is required. This uncertainty can be attributed to a lot of unaccounted factors, e.g., real lag changes, underestimated observational uncertainties, etc. The likelihood method is widely used for constructing estimators of unknown parameters in statistics. Maximum-likelihood estimation was vastly popularized by Ronald Fisher (e.g. Fisher 1912). In our implementation of this method, an additional lag scattering σ is unknown parameter to be found by achieving a maximum of the function:

$$L(\sigma) = \prod_{i=1}^3 \rho_i(\tau = \tau_0, \sigma),$$

where the index i represents one of the three observing periods, and $\rho_i(\tau, \sigma)$ is a convolution of the two probability distributions of τ : one is obtained from the FR/RSS technique

for a given period (see Fig. 6), while another is a normal distribution with unknown standard deviation σ and with the expectation equals to the mean lag τ_0 from the last column of Table 5. Such a method provides larger lag uncertainties than the FR/RSS technique does. E.g., the uncertainties in the mean lag can even be greater than the uncertainties for individual periods of observations when there is a large scattering in individual lag values. The additional uncertainty in the lag between the continuum and H β emission was found to be $\sigma = 13$ d.

3.4 Central black hole mass

The reverberation mass of the central black hole is given by

$$M_{BH} = \frac{f c \tau \sigma_{line}^2}{G},$$

where G is the gravitational constant, c is the light velocity, τ is the emission-line time delay (a proxy for the BLR size), σ_{line} is the width of this line (a proxy for the velocity dispersion of BLR gas), and f is the scaling factor of order unity that depends on the BLR geometry, kinematics, and orientation. To obtain the M_{BH} directly in the Solar mass units, the above equation can be written as

$$M_{BH} = \frac{k \tau \sigma_{line}^2}{1.14 \times 10^{-10}}, \quad (3)$$

where $k \equiv 2f$, σ_{line} is in light-velocity units, τ is in days, and 1.14×10^{-10} is gravitational radius of Sun in light-days. Here we adopt a definition for the gravitational radius r_g according to Oppenheimer & Snyder (1939) (the same definition was used in Sergeev et al. 2002, 2011), i.e., $r_g = 2GM/c^2$.

While it is difficult to determine f for an individual source because dynamical modeling is required, its average value has been determined by comparing the available reverberation measurements with the measurements from the well known $M_{BH} - \sigma_*$ relationship for AGNs. The most recent determination of the scale factor for reverberation-mapped AGNs is $f = 4.31 \pm 1.05$ (Grier et al. 2013) and it is consistent with earlier results (e.g., Onken et al. 2004; Graham et al. 2011). As in Sergeev et al. (2011) we adopt f to be 5.5 according to Onken et al. (2004).

Recent results of observations obtained with high sample rate show the diversity and probable complexity of the BLR velocity field (Denney et al. 2009, 2010; Grier et al. 2012) with indications of outflowing component at least for NGC 3227 nucleus. Since the reverberation method is based on the virial assumption, it does call into question the reliability of this method for the determination of black hole masses.

The line width is usually measured as FWHM or line dispersion σ_{line} (i.e. the second moment of the line profile). It has been argued that σ_{line} is a less biased measure of the velocity dispersion of BLR gas than FWHM (e.g., Sergeev et al. 1999; Collin et al. 2006). Similarly, it was argued that the τ_{cent} above the correlation coefficients of $0.8r_{max}$ is the most representative lag estimate for the BLR radius (Peterson et al. 2004). It seems, from our experience, that the τ_{cent} distribution is more normal with slightly less deviations than that of τ_{peak} . Estimates of τ_{cent} above lower correlation levels seem to be not applicable because far CCF wings are poorly determined since a limitation on time shift. Note that a significant difference between the τ_{peak} and τ_{cent} is only pronounced if the BLR is strongly extended spatially, so the transfer function has a long tail.

In Table 6 we give the H α and H β broad-line widths and centroids (narrow emission-lines are removed from the broad profiles) for the three periods of observations: 1993–1997, 2005–2007, and 2008–2014. They were computed from both the mean and rms profiles and for the same time intervals as that of the time lag computations. The uncertainties in σ_{line} were computed as described in Sergeev et al. (2011) and they were found to be about 5 per cent for all observing periods, while the uncertainties in the centroids were found to be 1.1 Å and 2.5 Å, for the H β and H α lines respectively.

As can be seen from Table 6, the σ_{line} value for both lines is remarkably constant among all periods. It seems that the widths of the Balmer lines in 3C 390.3 (as well as their lags, see Table 5) depend little, if any, on the continuum flux that was much brighter in 2005–2014 than in 1993–1997.

Also seen from Table 6 is that the H α and H β broad-line centroids have shifted to shorter wavelengths between 1993–1997 and 2005–2014 because systematic brightening of the blue bump of the line profiles. There were no changes in the centroids between 2005–2007 and 2008–2014 for both the H α and H β lines except for the rms profile of the H α line that is shifted to longer wavelengths.

To compute the average mass for the three observational periods we adopt the σ_{line} value for the rms profiles to be a mean value among three periods (note, that these three values are almost the same). The mean σ_{line} value for the three periods from Table 6 is equal to 4557 and 4143 km s^{−1}, while the mean τ_{cent} value is equal to 88.6 ± 8.4 and 161 ± 15 d (see last column of Table 5) for the H β and H α lines, respectively. The lag values need to be corrected for time dilation by dividing by $1 + z$ to put them into the rest frame. After correction for time dilation (assuming $z = 0.05553$) the corresponding estimates of the black hole mass in 3C 390.3 are $(1.87 \pm 0.26) \times 10^9 M_{\odot}$ and $(2.81 \pm 0.38) \times 10^9 M_{\odot}$ under $f = 5.5$. Here we have conservatively adopted the uncertainties in the mean width of both lines to be equal to the uncertainties for the individual periods, i.e. 5 per cent. Note, that the reverberation mass uncertainties originate not only from the observational uncertainties and data sampling, but

from the uncertainties in the scale factor f , and from the validity of the virial assumption for a given emission-line in a given AGN.

As was shown by Sergeev et al. (1999) the coefficient k in eq. 3 is approximately equal to $4/\sin^2 i$ for the Keplerian disc model, where i is the inclination angle ($i = 0^\circ$ for pole-on configuration). Assuming the BLR in the 3C 390.3 nucleus to be a Keplerian disc with $i = 27.6^\circ$ (see Sergeev et al. 2002), the expected value of the scale factor is $f \approx 9.3$. If so, our reverberation mass must be enlarged by a factor of $9.3/5.5 = 1.7$. Indeed the model-dependent mass estimate in sect. 3.5 gives a larger black hole mass in 3C 390.3.

Wandel, Peterson, & Malkan (1999) and Dietrich et al. (2012) claimed the central black hole in 3C 390.3 to be $4 \times 10^8 M_{\odot}$ and $8.6 \times 10^8 M_{\odot}$, respectively. This is several times less than our mass estimate. Except for a difference in both the adopted scale factor and in the adopted method to measure the line width, the principal reason for above disagreement is a disagreement in the measured H β lag. This lag was found to be 24 days and 44 days in Wandel, Peterson, & Malkan (1999) and in Dietrich et al. (2012), respectively. Sergeev et al. (2002) have argued that this disagreement in the lag must be attributed to the broader ACF width for our time series (see also Netzer & Maoz 1990, to learn more about how the ACF width affects lag measurements). The ACF width is expected to be systematically greater for a longer observing campaign because long-term program shows variability timescales not sampled in the short-term campaign. Our monitoring campaign is definitely longer than that of Wandel, Peterson, & Malkan (1999) and Dietrich et al. (2012) (about one year and several months, respectively). In contrast to the short-term campaigns above, the multi-year campaigns give the H β lag in 3C 390.3 to be comparable to our lag estimate. Thus Shapovalova et al. (2010) claimed a lag of 95 days for the H β line and 120 days for the H α lines, while Afanasiev et al. (2015) found this lag to be 60–79 and 138–186 days, respectively. It is clear that the mass of the black hole determined from above lags (the authors did not calculate the mass) should be in agreement with our mass estimate.

The central black hole mass in 3C 390.3 was found to be $(5 \pm 1) \times 10^8 M_{\odot}$ from the stellar velocity dispersion (Lewis & Eracleous 2006), again less than our mass estimate. This disagreement can be attributed to the intrinsic scattering in the $\sigma_* - M_{BH}$ relationship as well as to uncertainties in the scale factor f . These uncertainties are related to the unknown geometry/kinematics and to a possible non-virial gas motions in the BLR.

Since our new τ_{cent} and σ_{line} measurements for 2008–2014 are almost the same as in Sergeev et al. (2011), it is not surprising that the mass estimates are almost the same as well, and that the 3C 390.3 nucleus is indeed an ‘outsider’ in the fundamental relationship between optical luminosity and black hole mass. Indeed, we found, from all observing periods, that the Eddington ratio is $E_{bol}/E_{Edd} = 0.0037$. Here we adopt $L_{bol} = 1.3 \times 10^{38} M_{BH}$ and $L_{Edd} = 9 \times \lambda L_{5100}$, where L_{bol} is the bolometric luminosity, L_{Edd} is the Eddington luminosity, and L_{5100} is the rest frame absolute luminosity of the 3C 390.3 nucleus at $\lambda = 5100 \text{ Å}$ (in units of ergs Å^{−1}). The bolometric luminosity has been corrected for Galactic reddening using $A_V = 0.22$ according to the red-

Table 6. H α and H β profile width.

Component	1993–1997			2005–2007			2008–2014		
	FWHM (km s ⁻¹)	σ_{line} (km s ⁻¹)	Centroid (Å)	FWHM (km s ⁻¹)	σ_{line} (km s ⁻¹)	Centroid (Å)	FWHM (km s ⁻¹)	σ_{line} (km s ⁻¹)	Centroid (Å)
H α mean	11380	4310	6932.0	10600	4180	6910.7	10490	4150	6909.5
H β mean	12690	4860	5143.8	12520	4280	5132.2	13740	4700	5132.3
H α rms	11570	4270	6935.8	8830	4010	6901.4	9480	4150	6922.5
H β rms	12010	4520	5142.2	12330	4530	5121.7	9460	4620	5123.6

Table 7. Determination of the black hole mass in terms of the Keplerian disc model

Years	M_{BH}	a	$\frac{\chi^2_{fit}}{dof}$	$P(\chi^2 > \chi^2_{fit})$
H β line fit				
1993–1997	2.2×10^9	0.80	4.47	2×10^{-22}
2005–2007	4.1×10^9	1.12	1.85	1.4×10^{-4}
2008–2014	1.9×10^9	0.68	4.29	0
1992–2014	3.2×10^9	0.71	14.2	0
1992–2014 ^a	2.5×10^9	0.77	4.77	0
H α line fit				
1993–1997	4.3×10^9	0.44	1.48	0.0072
2005–2007	6.1×10^9	1.04	0.49	0.923
2008–2014	4.2×10^9	0.43	1.76	0.0086
1992–2014	9.4×10^9	0.54	4.08	0
1992–2014 ^a	4.1×10^9	0.54	1.40	0.0016

^a With a long timescale trend removed, see text.

dening map from Schlegel, Finkbeiner, & Davis (1998) and it was found to be $L_{bol} = (1.01 \pm 0.25) \times 10^{44}$ ergs.

3.5 Model-dependent black hole mass

In Sergeev et al. (2011) the black hole mass in 3C 390.3 has been derived in terms of the relativistic Keplerian disc model of BLR (e.g., Chen et al. 1989; Eracleous & Halpern 1994). The disc parameters (the inner/outer radii, inclination angle, and emissivity law per unit surface) were taken from Sergeev et al. (2002). The free parameters are: the black hole mass M_{BH} , the power-law index a , and a scale factor c (see Sergeev et al. 2011, for more details). These parameters were obtained by fitting of modeled light curves of the H β and H α emission-lines to the observed light curves. It was assumed that the source of the continuum that drives the line is slightly above a disc centre (so its height is much less than the disc internal radius) and both the line and the optical continuum fluxes are power-law functions of the driving continuum fluxes, so the relationship between the line fluxes and optical continuum fluxes is a power-law as well: $F_{line} = cF_{cont}^a$. We select optical continuum light curve to be F_{5100} (see Fig. 2, top panel). In Table 7 we give the fit results for our new data set in 2008–2014 as well as for earlier periods and for the entire period of 1992–2014. Note that the masses in Table 7 should be divided by $1 + z$ because observed light curves are not corrected for time dilation.

From the inspection of the Table 7 the same conclusions as from the respective table in Sergeev et al. (2011) can be made, namely:

- (i) The fit quality in term of the χ^2 is too poor in many

cases, especially for the entire period of observations, so the probability computed from the high tail of χ^2 distribution (see the last column of Table 7) is too low. The lower χ^2 values for the H α line is mostly due to larger uncertainties of its light curve.

- (ii) There is a discrepancy in determination of the M_{BH} between H α and H β lines as well as between 1993–1997 and 2005–2007.

- (iii) The H α line shows lower values of the power-law index a as compared to the H β line, except for 2005–2007 when the responses of both lines to the optical continuum variations seem to be almost linear.

As was shown by Sergeev et al. (2011), the line responses to the variations of the continuum fluxes are non-linear (except for 2005–2007), especially for the H α line.

To improve the fit quality for the entire period, we assumed that there is a long-term trend in the line–continuum relationship. The long-term changes in this relationship were found, for example, by Malkov et al. (1997). To account for such changes, Denney et al. (2010) have proposed to use low-order polynomials to remove long-term trends from the light curves before applying cross-correlation analysis. We supposed that the poor fit quality for the entire period is related to the slow changes in the scale factor c , so that this factor is a function of time and $F_{line} = c(t)F_{cont}^a$. To remove this effect the fit procedure has been modified as follows: (1) the modeled light curve is divided by the observed light curve; (2) the division result is smoothed by convolution with the Gaussian function with $\sigma = 1$ year; (3) the modeled light curve is divided by the smoothed curve to represent the observed light curve. The large improvement of the modified fit for the entire period is clearly seen from the Table 7: the χ^2 values per d.o.f decrease from 14.2 to 4.77 for the H β line and from 4.08 to 1.40 for the H α line. In Fig. 7 we show both the modeled and observed light curves of the H β line and the normalized scale factor $c(t)$ for both H α and H β lines. There is a close similarity between both scale factors. They have reached a minimum in 2004, i.e., approximately at the beginning of the systematic continuum brightening.

Long-term variations of the scale factor can be interpreted, for example, via changes in the height of the driving continuum source above the disc centre. In terms of the considered disc model, the incident flux of the driving continuum has to be proportional to the height of its source for distances much exceeding this height.

Even after the modified fit is applied, the χ^2 values for both lines are significantly greater than their expected values. There are a lot of reasons for it, e.g.: (1) the considered disc model is too oversimplified or it is not correct; (2) the

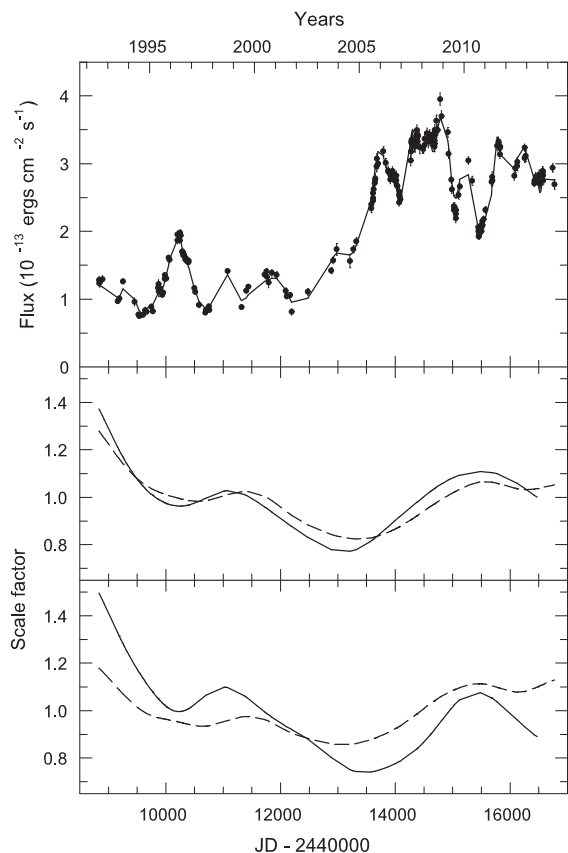


Figure 7. Observed H β light curve is shown by filled circles in the top panel. The fit to this curve in terms of the Keplerian disc model (see text) is shown by solid line. The middle and bottom panels show long-term changes in the scale factor c in the relationship $F_{line} = c F_{cont}^a$ between line and continuum fluxes for the H β and H α lines (dashed and solid lines, respectively). The middle panel shows this factor as obtained from the Keplerian disc model, while the bottom panel shows this factor as obtained from the model-independent calculations (see text).

long-term changes in the line–continuum relationship can be more complex than it is proposed and this relationship is not necessary to be a power-law; (3) the observational uncertainties can be underestimated; and (4) there are effect of gaps in the continuum light curve. In particular we found that the reasonable filling the largest gaps in the continuum light curve (made by eye) reduces the χ^2 per d.o.f. value for the H β line from 4.77 to 3.45.

We have verified whether similar long-term variations in the scale factor can be obtained by a model-independent way and how much these variations affect the cross-correlation results for the entire observational period. We used a modified cross-correlation function in which the continuum light curve is adjusted to the line light curve by the same method as in our modified fitting procedure except for the modeled light curve of a line is now the continuum light curve shifted by a given time lag. So, for each lag value we must perform the adjustment before compute the correlation coefficient. We computed the cross-correlation function between F_{line} and F_{cont}^a for a set of power-law indices a in order to find a largest r_{max} value. We found that the power-law in-

dices of 0.67 and 0.66 provide largest r_{max} values for the H β and H α lines, respectively. For above indices, the τ_{cent} value was found to be 80^{+4}_{-4} d for H β and 164^{+12}_{-16} d for H α with r_{max} values equal to 0.984 and 0.981, respectively. The cross-correlation function with no correction for the variations in the scale factors but with the power-law version of the continuum light curve gives the τ_{cent} value of 95 d with $r_{max} = 0.954$ for the H β line and of 190 d with $r_{max} = 0.939$ for the H α line. For linear relationship between line and continuum fluxes, the cross correlation results are as follows: $\tau_{cent} = 101$ d and $r_{max} = 0.942$ for the H β line and $\tau_{cent} = 194$ d and $r_{max} = 0.938$ for the H α line. Because CCFs for both lines for the entire time interval is too flat-top the centroid at $0.8 r_{max}$ can not be computed. Instead, to integrate over lag values, we used the lag intervals comparable to that for individual periods (about 160 and 320 days for the H β and H α , respectively). These intervals correspond to about $0.96 r_{max}$. Note a decrease in the derived lags and a significant increase in the correlation for both lines after accounting for variations in the scale factors.

Our Keplerian disc model gives the correlation coefficients between observed and modeled light curves of 0.990 and 0.988 for the H β and H α lines, larger than the correlation coefficients of the modified CCF above.

The derived scale factors $c(t)$ for both lines are shown in the bottom panel of Fig. 7. There is a similarity between scale factors from the Keplerian disc model and from the model-independent calculations.

3.6 Balmer decrement

As was found in Sergeev et al. (2011) the H α to H β ratio of fluxes ($F(H\alpha)/F(H\beta)$) varies with the continuum flux because the power-law index a is different between H α and H β lines. In Fig. 8 we show, in log-log scale, the $F(H\alpha)/F(H\beta)$ (top panel) and the $F(H\beta)/F(H\gamma)$ (bottom panel) ratios as functions of the optical continuum flux F_{5100} . Note that the H γ measurements are only available since 2005. Contributions from the host galaxy and from the narrow lines are subtracted. The time delays were taken into account by the respective time shifts of the light curves. The shifted light curves have been rebinned: the H β fluxes are rebinned to the times of observations of the H α fluxes, while the H γ fluxes are rebinned to the times of observations of the H β fluxes. The ordinary linear regression gives: $F(H\alpha)/F(H\beta) \propto F_{5100}^{-0.20}$ and $F(H\beta)/F(H\gamma) \propto F_{5100}^{-0.18}$. It seems that both relationships are not power-law exactly (i.e., not linear in the log-log scale) or there are long-term changes in these relationships. In the middle panel of the Fig. 8 we show the $F(H\alpha)/F(H\beta)$ ratio vs. F_{5100} as expected from our Keplerian disc model where the long-term changes in the scale factors for both lines are accounted for. The expected relationship is linear (in log-log scale) with relatively small deviations of individual data points. This is different from the observed relationship (top panel of Fig. 8). Probably the power-law approximation to the relationship between Balmer line and continuum fluxes is not exactly correct.

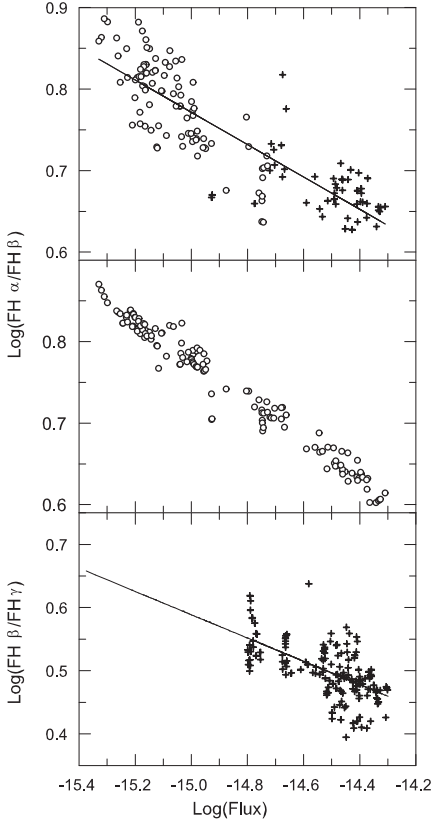


Figure 8. Balmer decrement ($F(\text{H}\alpha)/F(\text{H}\beta)$ and $F(\text{H}\beta)/F(\text{H}\gamma)$) vs. optical continuum flux ($\text{ergs cm}^{-2} \text{s}^{-1} \text{\AA}^{-1}$). The scale is logarithmic on both axes. Open circles indicate observations in 1992–2002, while crosshair symbols are the observations since 2003 when a systematic continuum brightening begins. The solid lines is the ordinary linear regression applied for entire period of observations. Middle panel shows Balmer decrement vs. optical continuum flux as expected from the Keplerian disc model (see text), while top and bottom panels show the observed Balmer decrement.

4 SUMMARY

(i) We confirm the variability of the narrow-line fluxes in the 3C 390.3 nucleus. The $[\text{O III}] \lambda 5007$ line flux increases monotonically by ≈ 30 per cent during about ten years in 2003–2014. The narrow Balmer lines show similar monotonic increase, while variability patterns of the $[\text{O I}] \lambda 6300$ narrow line are completely different from that of $[\text{O III}]$. The observed variability of the $[\text{O III}] \lambda 5007$ line fluxes can be reproduced, for example, in terms of the transfer function of the spherically symmetric shell with the inner and outer radii of 20 and 150 light-years, respectively, and the $[\text{O III}]$ emissivity per unit volume $\varepsilon \propto r^{-3.5}$.

(ii) The mean lags for the three periods of observations were found to be 88.6 ± 8.4 , 161 ± 15 , and 113 ± 14 d for the $\text{H}\alpha$, $\text{H}\beta$, and $\text{H}\gamma$ broad emission-lines, respectively ($\text{H}\gamma$ line measurements are only available for the last two periods). These values need to be corrected for time dilation by dividing by $1+z$ to put them into the rest frame.

(iii) It seems that the lags of the Balmer lines depend little, if any, on the continuum flux.

(iv) The mean reverberation mass of the central black hole in the 3C 390.3 nucleus was found to be $(1.87 \pm 0.26) \times 10^9 M_\odot$ and $(2.81 \pm 0.38) \times 10^9 M_\odot$, for the $\text{H}\beta$ and $\text{H}\alpha$ broad emission-lines and under $f = 5.5$.

(v) The black hole mass estimates from both lines are different at 2σ confidence. Probably, there is a difference between kinematics of the $\text{H}\alpha$ and $\text{H}\beta$ emission regions which translates to a difference in the value of the scale factor f as was suggested by Sergeev et al. (2011).

(vi) The Keplerian disc model we consider in the present paper and the model-independent calculation both show that the reverberation mapping can only be applied to the entire (more than twenty years) period of observations of the 3C 390.3 nucleus after removing a long-term trend. This trend has been expressed by a variable scale factor $c(t)$ in the power-law relationships between line and continuum fluxes: $F_{\text{line}} \propto c(t) F_{\text{cont}}^a$. In terms of the Keplerian disc model, the origin of this trend can be attributed to the changes in the height of the driving continuum source above the disc centre.

(vii) The responses of the $\text{H}\alpha$, $\text{H}\beta$, and $\text{H}\gamma$ broad emission-lines in 3C 390.3 to the optical continuum variations are non-linear. According to our Keplerian disc model the power-law index a equals to 0.77 and 0.54 for the $\text{H}\beta$ and $\text{H}\alpha$ lines, respectively. Since the power-law index a is different among Balmer lines, the Balmer decrement must vary with the continuum flux. The observed relationship between this decrement and the optical continuum flux is as follows: $F(\text{H}\alpha)/F(\text{H}\beta) \propto F_{\text{cont}}^{-0.20}$ and $F(\text{H}\beta)/F(\text{H}\gamma) \propto F_{\text{cont}}^{-0.18}$. It seems that the relationship between Balmer line and continuum fluxes is slightly different from the power-law function.

(viii) We confirm that the 3C 390.3 nucleus is definitely an ‘outsider’ in the fundamental relationship between optical luminosity and black hole mass. Its Eddington ratio of $E_{\text{bol}}/E_{\text{Edd}} = 0.0037$ is very low.

ACKNOWLEDGMENTS

The CrAO CCD cameras have been purchased through the US Civilian Research and Development Foundation for the Independent States of the Former Soviet Union (CRDF) awards UP1-2116 and UP1-2549-CR-03.

REFERENCES

- Afanasiev V. L., Shapovalova A. I., Popović L. Č., Borisov N. V., 2015, MNRAS, 448, 2879
- Barr P., et al., 1980, MNRAS, 193, 549
- Bentz M. C., et al., 2009, ApJ, 705, 199
- Bentz M. C., et al., 2010, ApJ, 716, 993
- Blandford R.D., McKee C.F., 1982, ApJ, 255, 419
- Burbidge E.M., Burbidge G.R., 1971, ApJ, 163, L21
- Chen K., Halpern J.P., 1989, ApJ, 344, 115
- Chen K., Halpern J.P., Filippenko A.V., 1989, ApJ, 339, 742
- Clavel J., Wamsteker W., 1987, ApJ, 320, L9
- Collin S., Kawaguchi T., Peterson B.M., Vestergaard M., 2006, A&A, 456, 75
- Denney K. D., et al., 2009, ApJ, 704, L80
- Denney K. D., et al., 2010, ApJ, 721, 715
- Dietrich M., et al., 1998, ApJS, 115, 185

- Dietrich M., et al., 2012, *ApJ*, 757, 53
- Doroshenko V. T., Sergeev S. G., Klimanov S. A., Pronik V. I., Efimov Y. S., 2012, *MNRAS*, 426, 416
- Doroshenko V. T., Sergeev S. G., Merkulova N.I., Sergeeva E.A., Golubinsky Yu.V., Pronik V.I., Okhmat N.N., 2005a, *Astrophysics*, 48, 156
- Eracleous M., Halpern J.P., 1994, *ApJS*, 90, 1
- Eracleous M., Livio M., Halpern J. P., Storchi-Bergmann T., 1995, *ApJ*, 438, 610
- Fisher R. A., 1912, *Messenger of Mathematics*, 41, 155
- Flohic H. M. L. G., Eracleous M., 2008, *ApJ*, 686, 138
- Gaskell C.M., Sparke L.S., 1986, *ApJ*, 305, 175
- Gezari S., Halpern J.P., Eracleous M., 2007, *ApJS*, 169, 167
- Graham A. W., Onken C. A., Athanassoula E., Combes F., 2011, *MNRAS*, 412, 2211
- Grier C. J., et al., 2012, *ApJ*, 755, 60
- Grier C. J., et al., 2013, *ApJ*, 773, 90
- van Groningen E., Wanders I., 1992, *PASP*, 104, 700
- Gültekin K., et al., 2009, *ApJ*, 698, 198
- Horne K., Peterson B.M., Collier S.J., Netzer H., 2004, *PASP*, 116, 465
- Kaspi S., Smith P.S., Netzer H., Maoz D., Jannuzi B.T., Givon U., 2000, *ApJ*, 533, 631
- Kovačević A., Popović L. Č., Shapovalova A. I., Ilić D., Burenkov A. N., Chavushyan V. H., 2014, *AdSpR*, 54, 1414
- Lewis K. T., Eracleous M., 2006, *ApJ*, 642, 711
- Lynds C.R., 1968, *AJ*, 73, 888
- Malkov Yu.F., Pronik V.I., Sergeev S.G., 1997, *A&A*, 324, 904
- Netzer H., 1982, *MNRAS*, 198, 589
- Netzer H., Maoz D., 1990, *ApJ*, 365, L5
- O'Brien P.T., et al., 1998, *ApJ*, 509, 163
- Onken C.A., Ferrarese L., Merritt D., Peterson B.M., Pogge R.W., Vestergaard M., Wandel A., 2004, *ApJ*, 615, 645
- Oppenheimer J. R., Snyder H., 1939, *PhRv*, 56, 455
- Osterbrock D.E., Koski A.T., Phillips M.M., 1976, *ApJ*, 206, 898
- Peterson B. M., 1993, *PASP*, 105, 247
- Peterson B. M., 1994, in *Gondhalekar P.M., Horne K., Peterson B.M., eds, ASP Conf. Ser. Vol. 69, Reverberation mapping of the broad-line region in active galactic nuclei. Astron. Soc. Pac., San Francisco*, p. 1
- Peterson B. M., et al., 2004, *ApJ*, 613, 682
- Peterson B. M., et al., 2013, *ApJ*, 779, 109
- Peterson B. M., Wanders I., Bertram R., Hunley J.F., Pogge R.W., Wagner R.M., 1998b, *ApJ*, 501, 82
- Peterson B. M., Wanders I., Horne K., Collier S., Alexander T., Kaspi S., Maoz D., 1998a, *PASP*, 110, 660
- Pronik I., Pronik V., 1992, *A&AT*, 3, 57
- Sandage A., 1966, *ApJ*, 145, 1
- Sergeev S. G., Doroshenko V.T., Golubinskiy Yu.V., Merkulova N.I., Sergeeva E.A., 2005, *ApJ*, 622, 129
- Sergeev S. G., Klimanov S. A., Doroshenko V. T., Efimov Y. S., Nazarov S. V., Pronik V. I., 2011, *MNRAS*, 410, 1877
- Sergeev S. G., Pronik V.I., Peterson B.M., Sergeeva E.A., Zheng W., 2002, *ApJ*, 576, 660
- Sergeev S. G., Pronik V.I., Sergeeva E.A., Malkov Yu.F., 1999, *AJ*, 118, 2658
- Sergeev S. G., Pronik V. I., Sergeeva E. A., 2000, *A&A*, 356, 41
- Shapovalova A. I., et al., 2001, *A&A*, 376, 775
- Shapovalova A. I., et al., 2010, *A&A*, 517, A42
- Schlegel D. J., Finkbeiner D. P., Davis M., 1998, *ApJ*, 500, 525
- Veilleux S., Zheng W., 1991, *ApJ*, 377, 89
- Wamsteker W., Wang T.-G., Scharrel N., Vio R., 1997, 288, *MNRAS*, 225
- Wandel A., Peterson B. M., Malkan M. A., 1999, *ApJ*, 526, 579
- White R.J., Peterson B.M., 1994, *PASP*, 106, 879
- Yee H.K.C., Oke J.B., 1981, *ApJ*, 248, 472
- Zheng W., 1996, *AJ*, 111, 1498
- Zheng W., Perez E., Grandi S. A., Penston M. V., 1995, *AJ*, 109, 2355